LHCHWG-2025-012, CERN-TH-2025-170, KA-TP-27-2025, P3H-25-062, SI-HEP-2025-18

State-of-the-art electroweak Higgs boson pair production in association with two jets at the LHC in the Standard Model and beyond

Jens Braun[1], Pia Bredt[2], Gudrun Heinrich,[1], Marius Höfer,[1], Barbara Jäger[3], Alexander Karlberg[4], Simon Reinhardt[3]

1 Institute for Theoretical Physics, Karlsruhe Institute of Technology (KIT), 76131 Karlsruhe, Germany
2 Department of Physics, University of Siegen, 57068 Siegen, Germany
3 Institute for Theoretical Physics, University of Tübingen, Auf der Morgenstelle 14, 72076 Tübingen, Germany
4 CERN, Theoretical Physics Department, 1211, Geneva 23, Switzerland

j.braun@kit.edu, pia.bredt@uni-siegen.de, gudrun.heinrich@kit.edu, marius.hoefer@kit.edu, jaeger@itp.uni-tuebingen.de, alexander.karlberg@cern.ch, simon.reinhardt@uni-tuebingen.de

Abstract

We present a systematic comparison of two state-of-the-art tools for the simulation of Higgs boson pair production via vector boson fusion (VBF) as implemented in the Monte-Carlo tools `GoSam+Whizard` and the `POWHEG-BOX`. Cross sections and distributions are provided within the Standard Model and beyond, within scenarios typical for experimental physics analyses, and for a range of energies of relevance to the LHC and its upcoming high luminosity phase. We further perform a detailed study of the so-called VBF approximation, in particular in the presence of anomalous Higgs boson couplings.

Received Date
Accepted Date
Published Date

Contents

1 Introduction

Following the discovery of the Higgs boson by the ATLAS [1] and CMS [2] Collaborations at the CERN Large Hadron Collider (LHC) in 2012, the particle physics community is now preparing for the upcoming high luminosity phase of the LHC (HL-LHC) [3]. One of the main objectives of this machine will be to precisely determine the couplings of the Higgs boson to the other particles of the Standard Model (SM) and, crucially, to itself [4]. One of the key production channels in this endeavour will be the vector boson fusion (VBF) Higgs boson pair production channel, which provides direct access to the Higgs boson self-coupling. Although the cross section of this process is smaller than the one for gluon fusion Higgs boson pair production by an order of magnitude, it provides a very clean experimental environment due to two energetic forward jets that accompany the Higgs boson pair.

From a theory point of view, VBF Higgs boson pair production in the SM is very well understood. Next-to-leading order (NLO) QCD corrections are sizeable (reaching $\mathcal{O}(30\%)$ in tails of distributions) and have been known in the *VBF approximation* (which is defined in detail in Section 2) for more than a decade [5–7]. They are available in the public codes `VBFNLO` [8–10] and `MadGraph5_aMC@NLO` [11]. Inclusive next-to-next-to-leading order (NNLO) QCD corrections in the same approximation (also known as factorizable NNLO corrections), were first calculated in Ref. [12], and have even been extended to next-to-next-to-next-to-leading order (N3LO) in Ref. [13]. Beyond the inclusive level, factorizable NNLO corrections are fully known [14] whereas non-factorizable corrections are only known in the leading eikonal approximation [15]. The publicly available code `proVBFHH` [16] contains all NNLO and N3LO

corrections.

In Ref. [17] the NLO electroweak (EW) corrections were computed and combined with NNLO QCD corrections, and the VBF approximation was studied.

Higgs boson pair production through VBF beyond the SM has been studied extensively in the literature using Effective Field Theories (EFTs) [18–23], and with the aim of distinguishing linear from non-linear realisations of the Higgs sector [24–29]. Apart from Ref. [22], none of the studies include NLO QCD corrections, and they do not offer NLO event generation.

Recently, two Monte Carlo programs that can provide NLO QCD corrections combined with the leading anomalous coupling contributions to this process have become available, one within the POWHEG framework [30], and another one based on GoSam+Whizard [31]. They differ mainly in their application of the VBF approximation. Whereas the POWHEG tool applies the VBF approximation, GoSam+Whizard retains all EW diagrams contributing to the $HHjj$ topology. This allows us to perform a detailed study of the VBF approximation also in the presence of both NLO QCD corrections and anomalous couplings.

In this paper we therefore carry out a comparative study of the two codes presented in Refs. [30, 31]. In Section 2 we define the process and the terminology, before identifying the leading anomalous couplings in the context of Higgs Effective Field Theory (HEFT). We briefly describe the technical aspects of the two tools in Section 3, and provide a range of results in the form of plots and tables of cross section values at $\sqrt{s} = 13, 13.6$ and 14 TeV in Section 4.1. In addition to predictions in the SM, we show cross sections at four benchmark points in the anomalous coupling parameter space. Section 4.2 is dedicated to the assessment of parton-shower effects and in Section 5 we conclude.

2 Electroweak Higgs boson pair production in association with two jets

In this paper we investigate the EW production of two Higgs bosons in association with two jets, i.e. the process $pp \to HHjj$ at $\mathcal{O}(\alpha^4)$, where α is the EW coupling constant. Neglecting the coupling of the Higgs boson to light quarks, there are two classes of contributions at the Born level to this process: on one hand the t-channel and u-channel scattering of two light quarks with the exchange of an EW vector boson, which radiates off the Higgs bosons (*VBF process*), and on the other hand the s-channel topology with a $q\bar{q}$ pair annihilating into an EW vector boson with subsequent decay into $q\bar{q}$ again (*Higgs strahlungs process*, see Fig. 1a). Interferences between t-channel and u-channel contributions as well as all s-channel contributions are known to be suppressed by the event selection cuts used in experiments [17, 32].The one-loop QCD corrections to the process then comprise all possible ways to attach a virtual gluon to the quark lines. The approximation keeping only t- and u-channel diagrams and neglecting their interference as well as all s-channel contributions is therefore usually referred to as the *VBF* approximation [32, 33]. In this approximation, NLO-QCD corrections to the upper and lower quark lines factorise. When instead including all contributions, we will speak of the *full process*. To suppress contributions from processes that are not of VBF type, typically so-called *VBF cuts* are applied on the invariant mass and the rapidity separation of the tagging jets. In some cases, such as signatures with several b-jets in the final state, experimental cuts are not in line with the VBF approximation, therefore the contributions of Higgs-strahlung-type can gain relative importance. Examples of diagrams not present in the VBF approximation are shown in Fig. 1. Note that, since in the full process all s-, t- and u-channel crossings and their interferences are taken into account, the contribution of diagrams such as in Fig. 1b does not vanish. This is different when only the t-channel and the u-channel contributions are considered separately, because of colour conservation. See Ref. [31] for more details.

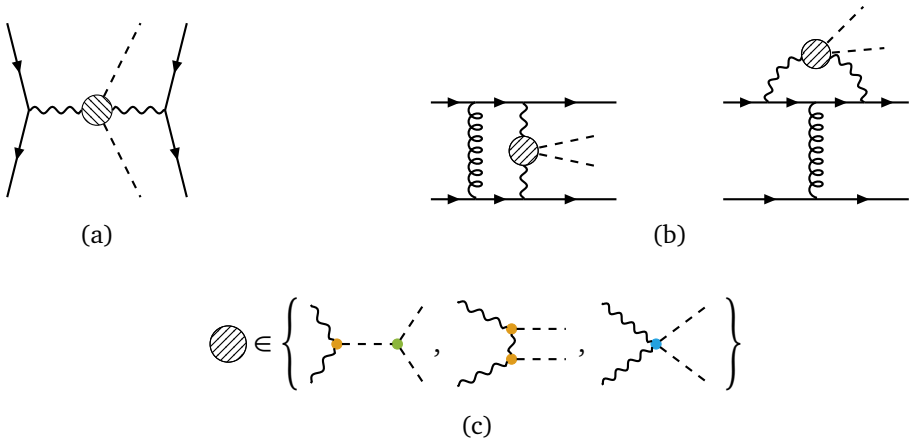

Figure 1: Examples of diagrams that are not included in the VBF approximation. The shaded blob in diagrams 1a and 1b can represent any of the sub-diagrams shown in 1c.

2.1 Higgs Effective Field Theory (HEFT)

While a full description of the framework of Higgs Effective Field Theory, also called HEFT or *Electroweak Chiral Lagrangian* [34–40], is beyond the scope of this paper, we briefly introduce some basic features here, such that we can identify the set of leading operators contributing to Higgs boson pair production in VBF.

In contrast to the Standard Model Effective Field Theory (SMEFT) [41–44], the Higgs field in the HEFT is not assumed to be part of a doublet of the electroweak $SU(2)$ symmetry. As a consequence, the Higgs field is treated independently from the Goldstone bosons and obeys fewer constraints than in the SMEFT. The EFT expansion is based on the so-called chiral dimension d_χ, which has a direct correspondence to the loop order L of a given operator, $d_\chi = 2L + 2$. The Lagrangian that is LO in the HEFT expansion collects all terms of chiral dimension $d_\chi = 2$, therefore we call it $\mathcal{L}_2$. The NLO (in the HEFT power counting) Lagrangian has chiral dimension $d_\chi = 4$, corresponding to loop order $L = 1$, and is denoted by $\mathcal{L}_4$. The main features of $\mathcal{L}_2$ are that the Higgs potential $V(h)$ can contain arbitrary powers of the Higgs field h, since h has chiral dimension zero,

$$V(\eta) = v^4 \sum_{n=2}^{\infty} V_n \eta^n \quad ; \quad \eta = \frac{h}{v}\,, \tag{1}$$

where v is the scale of electroweak symmetry breaking and V_n are $\mathcal{O}(1)$ coefficients. The term in the Lagrangian containing the covariant derivatives contains the so-called *flare function*,

$$F(\eta) = 1 + \sum_{n=1}^{\infty} F_n \eta^n\,, \tag{2}$$

where F_n are $\mathcal{O}(1)$ coefficients, such that the part of $\mathcal{L}_2$ containing the interactions of the Higgs boson with the gauge and Goldstone bosons reads

$$\mathcal{L}_2^{\text{gauge}-\text{Higgs}} = \frac{v^2}{2}\partial_\mu\eta\,\partial^\mu\eta - V(\eta) + \frac{v^2}{4}\left\langle (D_\mu U)^\dagger (D^\mu U)\right\rangle F(\eta)\,, \tag{3}$$

with

$$D_\mu U = \partial_\mu U + igW_\mu U - ig' B_\mu U t^3\,, \tag{4}$$

and $U = \exp(2i\varphi/v)$, where $\varphi = \varphi^\alpha t^\alpha$ with $\alpha = 1,2,3$ are the Goldstone boson fields and the t^α are the generators of the $SU(2)_L$ gauge group. $W_\mu = W_\mu^\alpha t^\alpha$ and B_μ denote the $SU(2)_L$ and $U(1)_Y$ gauge fields, respectively, with associated gauge couplings g and g'. The gauge-fermion interactions remain SM-like at LO in the HEFT expansion. We omit contributions to $\mathcal{L}_2$ that violate custodial symmetry because they would generate a tree-level contribution to the electroweak ρ-parameter, which would have been noticed experimentally [45, 46].

Finally, we note that the process, within the VBF approximation, in the context of the SMEFT could in principle be studied using the MadGraph5_aMC@NLO [7] framework in conjunction with SMEFT@NLO [47]. However, to our knowledge such a study has never been published.

2.2 Effective HEFT Lagrangian for Higgs boson pair production in VBF

Focusing on Higgs boson pair production in VBF, the leading anomalous interactions resulting from $\mathcal{L}_2$ can be parametrised as follows:

$$\mathcal{L}_{\text{eff}} \supset \left(2c_V\frac{h}{v} + c_{2V}\frac{h^2}{v^2}\right)\left(m_W^2 W_\mu^+ W^{-\mu} + \frac{1}{2}m_Z^2 Z_\mu Z^\mu\right) - c_\lambda \frac{m_h^2}{2v}h^3\,, \tag{5}$$

where $W_\mu^\pm = (W_\mu^1 \mp W_\mu^2)/\sqrt{2}$ and $Z_\mu = \cos\theta_W W_\mu^3 - \sin\theta_W B_\mu$, with θ_W the Weinberg angle just as in the SM. Note that no new structures arise which are not present in the SM and that for $c_V = c_{2V} = c_\lambda = 1$ we recover the SM. Operators from $\mathcal{L}_4$ are not included in this analysis, which we motivate by the fact that we focus on the NLO QCD corrections. In principle, performing a calculation beyond tree level implies that also operators with chiral dimension $d_\chi = 4$, i.e. one-loop order, have to be considered, because tree-level amplitudes with a single vertex insertion from $\mathcal{L}_4$ are of the same order as genuine one-loop amplitudes constructed from interactions contained in $\mathcal{L}_2$ only. However, here we restrict ourselves to NLO in QCD, which means that the one-loop corrections are $\mathcal{O}(\alpha_s)$ in the strong coupling α_s relative to the Born contributions. These Born contributions are $\mathcal{O}(\alpha^4)$ in the EW coupling α for Higgs boson pair production in VBF. Thus, in our NLO QCD calculation, we include all coupling powers at $\mathcal{O}(\alpha^4\alpha_s)$. Although the HEFT operators do not exhibit explicit powers in either the electroweak or strong coupling, one can still make a formal assignment based on their possible couplings to SM particles in a renormalisable UV completion. Furthermore, from power counting arguments, it follows that each Higgs boson introduces a factor of $1/v \propto \sqrt{4\pi\alpha}$. Therefore, if SM NLO EW corrections were included in the calculation, this would require us to also consider operators from $\mathcal{L}_4$, to be consistent in the HEFT power counting.

2.3 The *kappa framework*

The effective Lagrangian from Eq. (5) coincides with the settings of the so-called *kappa framework* [48, 49], a simple prescription to parametrise deviations from the SM. Of course, this coincidence only holds as long as no NLO electroweak corrections are considered, and if the HEFT expansion is cut at chiral dimension $d_\chi = 2$, and if operators that violate custodial symmetry are neglected [31]. In the kappa framework, a coupling modifier κ_i is defined as the ratio of a coupling g_i to the corresponding SM coupling g_i^{SM}. In particular, the couplings of the Higgs boson entering the VBF-induced $HHjj$ production are given by

$$g_{HVV} = \kappa_V \cdot g_{HVV}^{\text{SM}}\,, \qquad g_{HHVV} = \kappa_{2V} \cdot g_{HHVV}^{\text{SM}}\,, \qquad g_{HHH} = \kappa_\lambda \cdot g_{HHH}^{\text{SM}}\,. \tag{6}$$

Here, g_{HVV} denotes the trilinear coupling of a Higgs boson to two massive weak bosons, g_{HHVV} the quartic coupling between two Higgs bosons and two massive weak bosons and g_{HHH} the trilinear Higgs coupling. In the following, we will express the coupling factors κ_i in terms of

the c_i introduced in Eq. (5), $\kappa_i = c_i$, and denote points in the parameter space of anomalous couplings in the format $[c_\lambda, c_V, c_{2V}]$.

3 Description of the Monte Carlo programs

3.1 GoSam+Whizard

GoSam [50–52] is a program package to produce and evaluate one-loop amplitudes in an automated way. It generates algebraic expressions for Feynman diagrams with the help of QGRAF [53] and FORM [54, 55]. Subsequently, integral reduction is performed using the tool NINJA [56, 57] and the master integrals are evaluated with ONELOOP [58]. It can import arbitrary model files written in the UFO format [59, 60]. The new version GoSam-3.0 [52] has additional EFT functionalities. Whizard [61, 62] is a multi-purpose Monte Carlo program providing phase space integration and event generation for hadron and lepton collider processes. It includes an automation of NLO SM corrections [63–65] relying on the FKS subtraction scheme [66]. The NLO events can be matched to a parton shower through an implementation of the POWHEG NLO matching scheme [67, 68] in Whizard [69, 70].

The amplitudes at the tree and one-loop level for the full EW $HHjj$ process are computed by GoSam and passed to Whizard via its interface based on the Binoth Les Houches Accord (BLHA) standard [71, 72].

The combined setup including EFT functionalities was first presented in [31] and is available at https://github.com/Jens-Braun/VBF_HH_HEFT.

3.2 POWHEG-BOX

The POWHEG-BOX [73] constitutes a general framework for the matching of fixed-order perturbative calculations with parton-shower (PS) programs using the POWHEG formalism [67, 68]. An implementation of the VBF-induced Higgs boson pair production process has been presented in [30] and is publicly available from the webpage of the POWHEG-BOX project at https://powhegbox.mib.infn.it/. This tool allows for the calculation of NLO-QCD corrections within the VBF approximation and their combination with multi-purpose Monte Carlo generators such as HERWIG [74] or PYTHIA [75]. At fixed order, both with and without anomalous couplings, it has been validated against the proVBFHH program [13–15]. In the following, we will refer to NLO-QCD predictions matched with a PS as NLO+PS results.

4 Results

We perform numerical studies for the three proton-proton centre-of-mass energies $\sqrt{s} = 13$, 13.6 and 14 TeV. For the discussion of differential distributions, we focus on the latter. We use the PDF4LHC21_40 set of parton distribution functions (PDFs) [76]. Jets are reconstructed with the anti-k_t algorithm [77] using a jet radius parameter of $R = 0.4$. As electroweak (EW) input parameters we choose the fine structure constant $\alpha(M_Z) = 1/127.9$, the Fermi constant, $G_F = 1.16637 \times 10^{-5}$ GeV^{-2}, and the mass of the Z boson, $M_Z = 91.1876$ GeV. This so-called “LEP-scheme" has been chosen since many electroweak precision observables (EWPOs) have been determined in this scheme. If EW corrections were included in our calculation, the W-mass would change in this scheme. The impact of different EW input schemes can be substantial, in particular in combination with EFT contributions [78]. However we focus on QCD corrections here, such that only the LO relations between the EW input parameters enter. The widths of the Z and W bosons are set to $\Gamma_Z = 2.4952$ GeV and $\Gamma_W = 2.085$ GeV,

respectively [46]. Throughout, we use a modified version of the complex mass scheme for massive gauge bosons $V = W^{\pm}, Z$, globally replacing their mass M_V^2 with $M_V^2 - iM_V\Gamma_V$, while keeping a real value for the EW couplings, see, e.g. Ref. [79] for more details. For the Higgs boson, we use a mass of $M_H = 125.09$ GeV and a width of $\Gamma_H = 3.7$ MeV. The factorisation and renormalisation scales, $\mu_F = \xi_F\mu_0$ and $\mu_R = \xi_R\mu_0$, are computed from the mass of the Higgs boson and the transverse momentum of the Higgs boson pair system, $p_{T,HH}$,

$$\mu_0 = \sqrt{\frac{M_H}{2}\sqrt{\frac{M_H^2}{4} + p_{T,HH}^2}}\,. \tag{7}$$

For the assessment of scale uncertainties, we perform a seven-point variation of the scale parameters ξ_F, ξ_R in the range 0.5 to 2. The scale choice above was first introduced in Ref. [14], and is based on a similar choice for single-Higgs that can be found in Ref. [80]. If one were to consider just the VBF approximation, the most natural scale choice would be to assign the virtuality, Q_1 or Q_2, of each of the exchanged vector bosons to their respective quark line. Since most Monte Carlo programs only assign a single scale to the event, a good choice is the geometric mean of the two vector boson virtualities, $\sqrt{Q_1Q_2}$. However, the vector boson virtuality is only well-defined in the strict VBF approximation. The idea behind the scale choice of eq. (7) is that it can be applied outside of the VBF approximation, and that it approximates $\sqrt{Q_1Q_2}$ reasonably well.

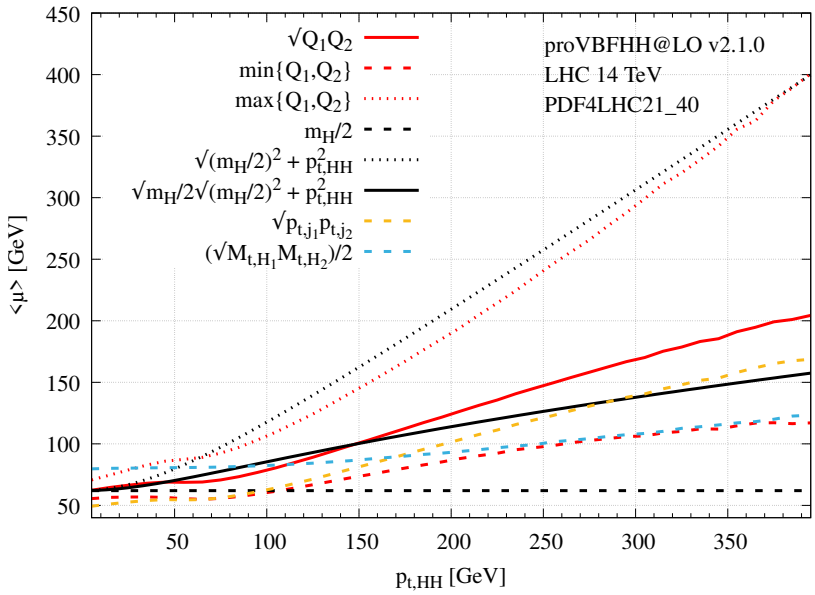

Figure 2: Various average scales as function of $p_{t,HH}$. In solid red we show $\sqrt{Q_1Q_2}$, in dashed and dotted red we show the minimum respectively the maximum of Q_1 and Q_2. In dashed black we show $m_H/2$, in dotted black $\sqrt{(m_H/2)^2 + p_{t,HH}^2}$, and in solid black the geometric mean of the two (the scale choice of this study). In dashed yellow we show the geometric mean of the transverse momentum of the two hardest jets, and in dashed light blue half the geometric mean of the transverse mass of the two Higgs bosons.

In Fig. 2 we illustrate this in the VBF approximation. The plot shows the average of various scales as a function of $p_{t,HH}$. The solid red line corresponds to the choice $\sqrt{Q_1Q_2}$, whereas the dashed respectively dotted lines correspond to the minimum and maximum of Q_1 and Q_2.

In dashed black $m_H/2$ is shown and in dotted black $\sqrt{(m_H/2)^2+p_{t,HH}^2}$. As can be seen they provide reasonable approximations for the true minimum and maximum. The scale choice of this study exactly corresponds to the geometric mean of $m_H/2$ and $\sqrt{(m_H/2)^2+p_{t,HH}^2}$. As can be seen from the plot this choice provides a very good approximation to $\sqrt{Q_1Q_2}$ in the range $p_{t,HH} \in [0:200]$ GeV, where the vast majority of the cross section lives, and even a reasonable approximation beyond. In dashed yellow and light blue we also show two alternative scales that are sometimes used, namely the geometric mean of the transverse momentum of the tagging jets, and half the geometric mean of the transverse mass of the Higgs bosons. Although both of these choices are parametrically of the same order as $\sqrt{Q_1Q_2}$ they fail to provide as satisfactory an approximation as eq. (7). For completeness we note that the picture above is qualitatively the same for single and di-Higgs VBF production.

Our default selection cuts are designed to favour VBF-induced $HHjj$ production. To that end we require the presence of at least two jets with transverse momenta and rapidities in the ranges

$$p_{T,j} > 25 \text{ GeV}, \quad |y_j| < 4.5\,. \tag{8}$$

The two hardest (highest transverse momentum) jets that meet these criteria are called *tagging jets*. On the tagging jets, we additionally impose requirements on their invariant mass and pseudorapidity separation,

$$m_{jj}^{\text{tag}} > 600 \text{ GeV}, \quad \Delta\eta_{jj}^{\text{tag}} = |\eta_{j_1}^{\text{tag}} - \eta_{j_2}^{\text{tag}}| > 4.5\,. \tag{9}$$

In the following we will refer to the cuts of Eqs. (8)–(9) as *VBF cut setup*, in contrast to an *inclusive cut setup*, where we only impose the cuts of Eq. (8).

Whenever we consider subleading jets, we require these to exhibit transverse momenta and rapidities in the ranges

$$p_{T,j_{sub}} > 25 \text{ GeV}, \quad |y_{j_{sub}}| < 4.5\,. \tag{10}$$

4.1 Assessment of the VBF approximation

The various tools presented in this work are designed to provide predictions for the VBF HH process within the SM and in the presence of anomalous Higgs couplings, including different subsets of perturbative contributions. To explore whether they are equivalently suited for the description of experimentally relevant scenarios, we have performed a detailed comparison of cross sections and characteristic differential distributions for different setups.

In Tabs. 1 and 2 we present results for cross sections of the EW $HHjj$ production process at LO and NLO-QCD accuracy obtained with the `GoSam+Whizard` and `POWHEG-BOX` programs for several values of the LHC centre-of-mass energy and the two cut scenarios introduced above. The benchmark points in the space of anomalous couplings shown in Tabs. 1 and 2 have been chosen such that they lead to characteristic shape changes in differential cross sections such as the invariant mass and rapidity of the di-Higgs system, see Ref. [31] for more details.

Because the `GoSam+Whizard` implementation includes the full EW $HHjj$ matrix elements, while the `POWHEG-BOX` implementation resorts to the VBF approximation, see section 2, differences between predictions obtained with the two programs are expected to be larger for inclusive setups than in VBF-specific phase-space regions.

Indeed, for the **inclusive cut** setup, we observe in Tab. 1 differences of almost 46% (30%) for the NLO (LO) cross sections for the SM predictions, and in the presence of anomalous couplings the differences can even exceed 50%. In contrast, for the **VBF cut** setup, the differences are at the one percent level both at LO and NLO, also in the presence of anomalous couplings,

$\sqrt{s} = 13\,\text{TeV}$	GoSam+Whizard		POWHEG-BOX		Ratio	
$[c_\lambda, c_V, c_{2V}]$	σ_{NLO} [fb]	K	σ_{NLO} [fb]	K	LO	NLO
$[1.0, 1.0, 1.0]$	1.387(10)	1.09	0.951(4)	0.97	1.295(3)	1.458(12)
$[-1.0, 0.9, 1.5]$	2.644(11)	1.02	2.381(7)	0.99	1.079(1)	1.110(6)
$[1.0, 0.9, 1.0]$	0.888(5)	1.14	0.508(2)	0.97	1.500(2)	1.748(12)
$[1.0, 1.0, 0.5]$	5.436(26)	1.00	5.168(9)	0.98	1.029(1)	1.052(5)
$[4.0, 0.95, 0.5]$	4.465(20)	1.05	3.459(7)	0.98	1.194(1)	1.291(6)
$\sqrt{s} = 13.6\,\text{TeV}$	GoSam+Whizard		POWHEG-BOX		Ratio	
$[c_\lambda, c_V, c_{2V}]$	σ_{NLO} [fb]	K	σ_{NLO} [fb]	K	LO	NLO
$[1.0, 1.0, 1.0]$	1.509(10)	1.08	1.055(6)	0.97	1.284(3)	1.430(12)
$[-1.0, 0.9, 1.5]$	3.021(12)	1.02	2.711(7)	0.99	1.077(1)	1.114(5)
$[1.0, 0.9, 1.0]$	0.988(5)	1.14	0.569(2)	0.97	1.481(2)	1.736(11)
$[1.0, 1.0, 0.5]$	6.009(26)	0.99	5.778(10)	0.98	1.028(1)	1.040(5)
$[4.0, 0.95, 0.5]$	4.982(24)	1.07	3.838(8)	0.98	1.188(2)	1.298(7)
$\sqrt{s} = 14\,\text{TeV}$	GoSam+Whizard		POWHEG-BOX		Ratio	
$[c_\lambda, c_V, c_{2V}]$	σ_{NLO} [fb]	K	σ_{NLO} [fb]	K	LO	NLO
$[1.0, 1.0, 1.0]$	1.587(11)	1.07	1.128(5)	0.97	1.277(3)	1.407(12)
$[-1.0, 0.9, 1.5]$	3.270(14)	1.02	2.942(7)	0.99	1.073(1)	1.111(5)
$[1.0, 0.9, 1.0]$	1.053(5)	1.14	0.614(2)	0.98	1.468(3)	1.715(10)
$[1.0, 1.0, 0.5]$	6.506(29)	1.00	6.208(11)	0.98	1.028(1)	1.048(5)
$[4.0, 0.95, 0.5]$	5.228(25)	1.05	4.104(9)	0.98	1.183(1)	1.274(7)

Table 1: Cross sections for the EW $HHjj$ production process at the LHC within the **inclusive cut** setup at NLO-QCD accuracy as obtained with the GoSam+Whizard and POWHEG-BOX programs for a selection of centre-of-mass energies, for the SM ($[1.0, 1.0, 1.0]$) and four benchmark points in the space of anomalous couplings. The numbers in parenthesis denote Monte Carlo integration uncertainties. The uncertainties of the K-factors (NLO/LO) are at permille level, i. e. one order of magnitude below the last K-factors' digit. The last two columns show the ratio GoSam+Whizard/POWHEG-BOX at LO and NLO, respectively.

as can be seen in Tab. 2. The dependence of the difference on the centre-of-mass energy is only marginal.

Let us emphasise that in typical VBF analyses where cuts are applied that enhance the relative contribution of VBF topologies to the full $HHjj$ production process, the use of tools relying on the VBF approximation is fully satisfactory. If, however, more inclusive selection cuts are applied, contributions neglected within the VBF approximation can become highly relevant, as we will investigate further in the following section by means of various differential distributions in the SM case.

4.1.1 Standard Model

As examples, in Fig. 3 we show distributions at $\sqrt{s} = 14\,\text{TeV}$ for the rapidity of the hardest tagging jet and for the transverse momentum of the hardest Higgs boson, respectively, illustrating the difference between the POWHEG-BOX and GoSam+Whizard predictions for the **inclusive cut** setup and the **VBF cut** setup, in the SM.

$\sqrt{s} = 13\,\text{TeV}$	GoSam+Whizard		POWHEG-BOX		Ratio	
$[c_\lambda, c_V, c_{2V}]$	σ_{NLO} [fb]	K	σ_{NLO} [fb]	K	LO	NLO
$[1.0, 1.0, 1.0]$	0.588(5)	0.92	0.585(2)	0.91	0.991(2)	1.005(9)
$[-1.0, 0.9, 1.5]$	1.614(8)	0.93	1.608(3)	0.92	0.998(1)	1.004(5)
$[1.0, 0.9, 1.0]$	0.284(2)	0.93	0.2862(9)	0.92	0.983(2)	0.992(8)
$[1.0, 1.0, 0.5]$	3.416(18)	0.92	3.395(6)	0.92	1.000(1)	1.006(6)
$[4.0, 0.95, 0.5]$	1.833(13)	0.93	1.806(5)	0.92	0.999(1)	1.015(8)
$\sqrt{s} = 13.6\,\text{TeV}$	GoSam+Whizard		POWHEG-BOX		Ratio	
$[c_\lambda, c_V, c_{2V}]$	σ_{NLO} [fb]	K	σ_{NLO} [fb]	K	LO	NLO
$[1.0, 1.0, 1.0]$	0.660(6)	0.93	0.654(2)	0.91	0.992(2)	1.009(10)
$[-1.0, 0.9, 1.5]$	1.846(10)	0.92	1.850(4)	0.92	0.998(1)	0.998(6)
$[1.0, 0.9, 1.0]$	0.320(3)	0.92	0.3253(9)	0.92	0.986(2)	0.984(10)
$[1.0, 1.0, 0.5]$	3.783(19)	0.90	3.826(7)	0.91	1.002(1)	0.989(5)
$[4.0, 0.95, 0.5]$	2.023(15)	0.91	2.034(5)	0.92	1.000(2)	0.995(8)
$\sqrt{s} = 14\,\text{TeV}$	GoSam+Whizard		POWHEG-BOX		Ratio	
$[c_\lambda, c_V, c_{2V}]$	σ_{NLO} [fb]	K	σ_{NLO} [fb]	K	LO	NLO
$[1.0, 1.0, 1.0]$	0.725(8)	0.95	0.704(2)	0.91	0.991(2)	1.030(12)
$[-1.0, 0.9, 1.5]$	2.042(11)	0.93	2.022(4)	0.91	0.996(1)	1.010(6)
$[1.0, 0.9, 1.0]$	0.347(3)	0.92	0.353(1)	0.92	0.981(2)	0.983(9)
$[1.0, 1.0, 0.5]$	4.179(22)	0.92	4.132(8)	0.91	1.002(1)	1.011(6)
$[4.0, 0.95, 0.5]$	2.162(16)	0.90	2.194(6)	0.92	1.002(2)	0.985(8)

Table 2: Cross sections for the EW $HHjj$ production process at the LHC within the **VBF cut** setup at NLO-QCD accuracy as obtained with the GoSam+Whizard and POWHEG-BOX programs for a selection of centre-of-mass energies, for the SM ($[1.0, 1.0, 1.0]$) and four benchmark points in the space of anomalous couplings. The numbers in parenthesis denote Monte Carlo integration uncertainties. The uncertainties of the K-factors (NLO/LO) are at permille level, i. e. one order of magnitude below the last K-factors' digit. The last two columns show the ratio GoSam+Whizard/POWHEG-BOX at LO and NLO, respectively.

We see clear differences for the **inclusive cut** setup, with factors of up to 2.5 (3.1) at LO (NLO) in the low-rapidity region and up to 1.7 (2.2) at LO (NLO) in the high p_{T,H_h} regime, with H_h being the hardest of the two Higgs bosons. These enhancements of differential cross sections with respect to the VBF approximation can be attributed to contributions of Higgs-strahlung diagrams which are pronounced especially in these regimes. Here the contribution of QCD corrections also dominantly comes from diagrams of Higgs-strahlung type which are not included in the VBF approximation results. This relation between the two different diagram selections can be also inferred by the total cross sections in Tab. 1, where the ratios in the last two columns are at about 1.3 (1.4) at LO (NLO) and the K-factors of `GoSam+Whizard` exceed those of `POWHEG-BOX` by about 10%.

For the **VBF cut** setup we only get differences of about 1% at LO for y_{j_1} and fairly good agreement at NLO in the range of the uncertainties, establishing the validity of the VBF approximation when VBF cuts are applied. Differences between the full process and the VBF approximation in the **VBF cut** setup are most pronounced in the tail of the p_{T,H_h} distribution, where the full process lies up to 7% below the VBF approximation at LO and up to 9% at NLO, fully consistent with Ref. [17]. Again this suppression in the tail can be attributed to increasing contributions of diagrams of Higgs-strahlung type. In contrary to the **inclusive setup**, the K-factor however can be observed to be approximately of the same size for both tools considering the complete range of y_{j_1} and p_{T,H_h}. The differential cross section is reduced by up to 19% in the low y_{j_1} region and 13% for low p_{T,H_h}, for both tools, which is also fully consistent with Ref. [17] within the **VBF cut** setup. This behaviour is also reflected in the K-factors in Tab. 2. The QCD corrections are thus found to contribute dominantly for diagrams of the pure VBF process.

We can conclude that in the **VBF cut setup** the effect of the NLO corrections on the distribution is covered well in the VBF approximation, i. e. $\mathcal{O}(\alpha_s)$ corrections to the full process beyond the approximation are much suppressed. Due to this observation and the fact that the ratios of total cross section in the last columns of Tab. 2 deviate from one at most by a few percent, for both LO and NLO, for all benchmark points of anomalous couplings, we only show LO results for the comparison beyond the SM in the next subsection.

4.1.2 Anomalous couplings

In Fig. 4 we display LO predictions at $\sqrt{s} = 14\,\text{TeV}$ for the rapidity y_{HH} and invariant mass m_{HH} of the di-Higgs system, respectively. We show results obtained with the `POWHEG-BOX` and `GoSam+Whizard` for the SM and different values for the anomalous coupling factors as listed in Tab. 2 within the **VBF cut** setup. We do not display results with anomalous couplings in the **inclusive cut** setup, because the differences between the full process compared to the VBF approximation exceed the differences due to the inclusion of anomalous couplings in the inclusive setup. We therefore only consider the **VBF cut** setup for this discussion. The anomalous couplings we have chosen are representative for characteristic shapes in differential cross sections while still being within experimental constraints [31, 81, 82].

For the **VBF cut** setup, we notice very good agreement between the two implementations, not only for the SM but also in the presence of anomalous couplings. The anomalous couplings lead to a significant change in the shape of the distributions compared to the SM, especially in the di-Higgs invariant mass distributions, while the rapidity distributions rather show overall shifts.

From the upper row of Fig. 4, we see that the VBF approximation only leads to differences at large rapidity of the di-Higgs system, which are not significant given the uncertainties, however.

For the di-Higgs invariant mass distribution, shown in the lower row of Fig. 4, the differences between the full process compared to the VBF approximation are in the 2% range, where

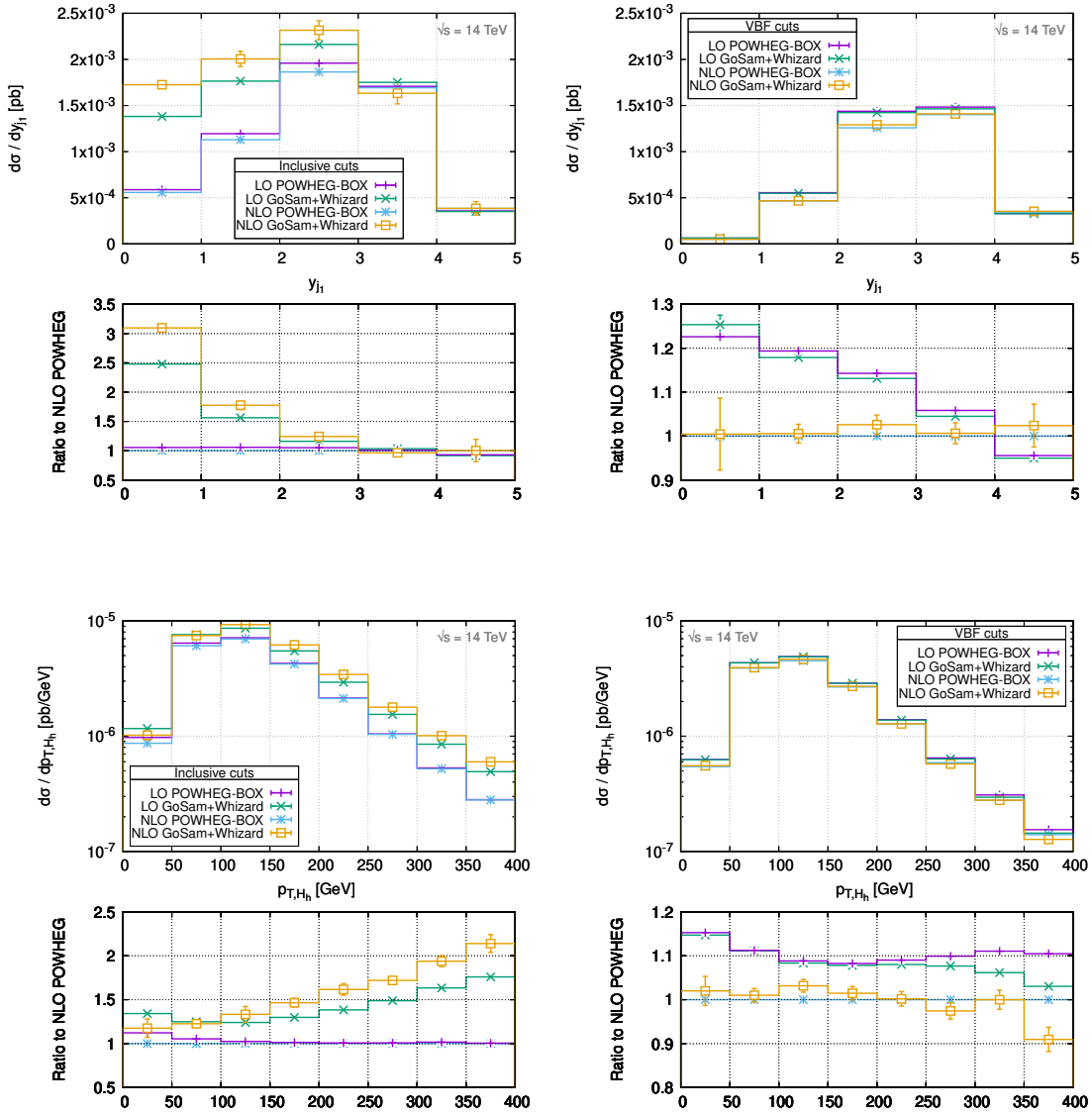

Figure 3: Distributions of the rapidity of the hardest tagging jet (top) and transverse momentum of the hardest Higgs boson (bottom) for the VBF HH process within the **inclusive cut** setup (left) and the **VBF cut** setup (right) as obtained with the POWHEG-BOX (LO: purple, NLO: blue) and GoSam+Whizard (LO: green, NLO: orange), and their ratios to the POWHEG-BOX results at NLO (lower panels).

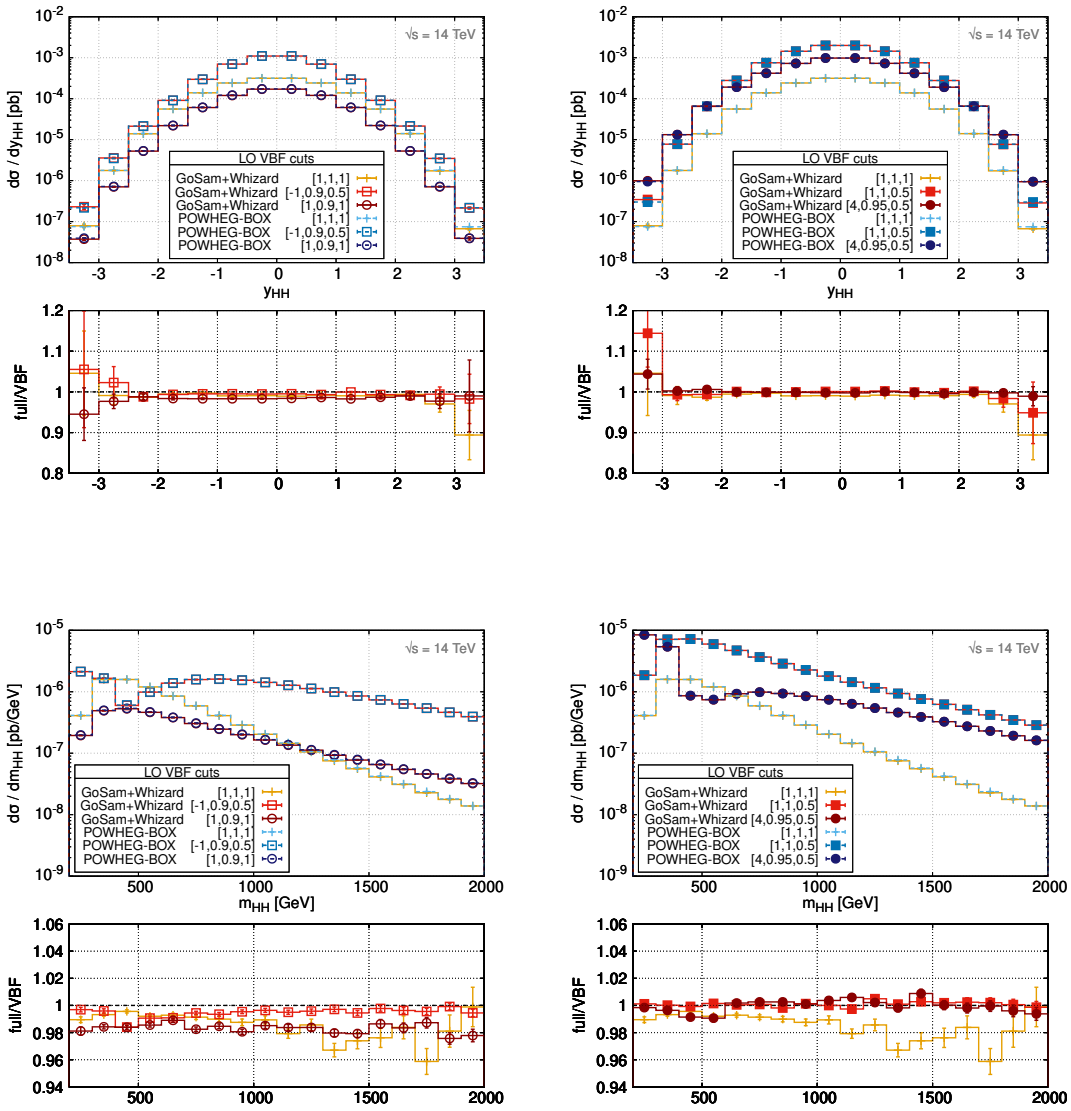

Figure 4: Rapidity (top) and invariant mass (bottom) distributions of the di-Higgs system for the VBF HH process within the **VBF cut** setup at LO as obtained with the `POWHEG-BOX` and `GoSam+Whizard` (upper panels), and the ratios of the full process (`GoSam+Whizard`) to the VBF approximation (`POWHEG-BOX`) for each set of anomalous couplings (lower panels). The values chosen for the anomalous Higgs couplings are quoted in the format $[c_\lambda, c_V, c_{2V}]$ for each curve in the legend. In addition to the SM results, denoted by $[1,1,1]$, predictions for the values $[-1, 0.9, 0.5]$ and $[1, 0.9, 1]$ are shown on the left, and for the values $[1, 1, 0.5]$ and $[4, 0.95, 0.5]$ on the right.

the full result tends to be slightly lower than the VBF approximation. However, changes in the value of c_{2V} (see for example point [1,1,0.5]) seem to shift the *full/VBF* ratio upward by a few percent compared to the SM ratio.

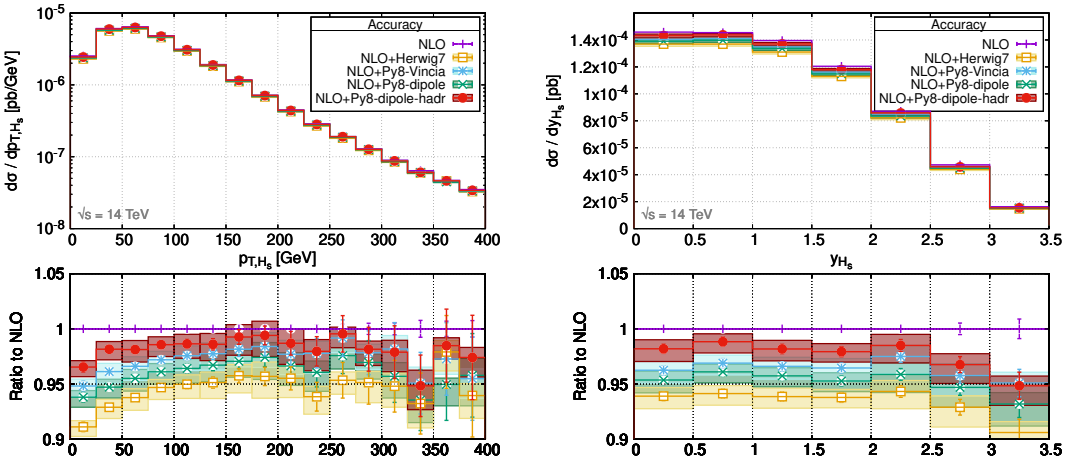

Figure 5: Transverse-momentum (left) and rapidity distributions (right) of the softer Higgs boson for the VBF HH process as described in the text within the **VBF cut** setup at NLO (purple) and at NLO+PS accuracy using HERWIG7 (orange) or PYTHIA8 with the dipole shower without (green) and with (red) hadronisation/underlying event effects, and the Vincia shower (blue). Their ratios to the respective NLO results are shown in the lower panels. Error bars indicate statistical uncertainties, uncertainty bands correspond to a 7-point variation around the central scale μ_0 of each curve.

4.2 Assessment of the impact of the parton shower

In order to assess the impact of parton-shower radiation on fixed-order results for the VBF HH process, we employ a selection of different multi-purpose Monte Carlo generators. For our default **VBF cut** setup with the cuts of Eqs. (8)–(9), we provide predictions obtained with our POWHEG-BOX implementation matching the NLO-QCD calculation with HERWIG7 (version 7.3.0) [74] and PYTHIA8 (version 8.312) [75] using the Monash tune [83]. For PYTHIA8 we consider both a local dipole shower and the Vincia antenna shower [84]. We note that using the global default shower of PYTHIA8 is not recommended for the simulation of VBF processes [85, 86], being unsuitable to account for the genuine radiation pattern. Underlying event and hadronisation are switched off unless specified otherwise.

Distributions of the tagging jets and the Higgs bosons do not exhibit a strong sensitivity to PS effects, as illustrated in Fig. 5 for the transverse momentum and rapidity of the softer Higgs boson, and in Fig. 6 for the azimuthal angle separation of the two Higgs bosons and the two tagging jets. Differences between predictions obtained with the various PS programs are small, with the Vincia NLO+PS curves being closest to the fixed-order NLO results. Including hadronisation effects results in a slight increase of the NLO+PS predictions.

Larger PS effects are observed for distributions of non-tagging jets. In particular, Fig. 7 illustrates the transverse-momentum and rapidity distributions of the third jet. Because of the cuts of Eq. (10), only jets with transverse momenta larger than 25 GeV contribute to these observables. NLO+PS results are several tens of percent below the respective NLO predictions, and the shape of both distributions changes considerably when PS radiation is taken into account, in particular in the central-rapidity region. We note that these large differences between NLO+PS and fixed-order results are reduced by the inclusion of NNLO corrections in the fixed-order calculation, see Ref. [30]. Even stronger changes in the shape of the third jet's rapidity distribution are obtained, if hadronisation effects are taken into account. In this case,

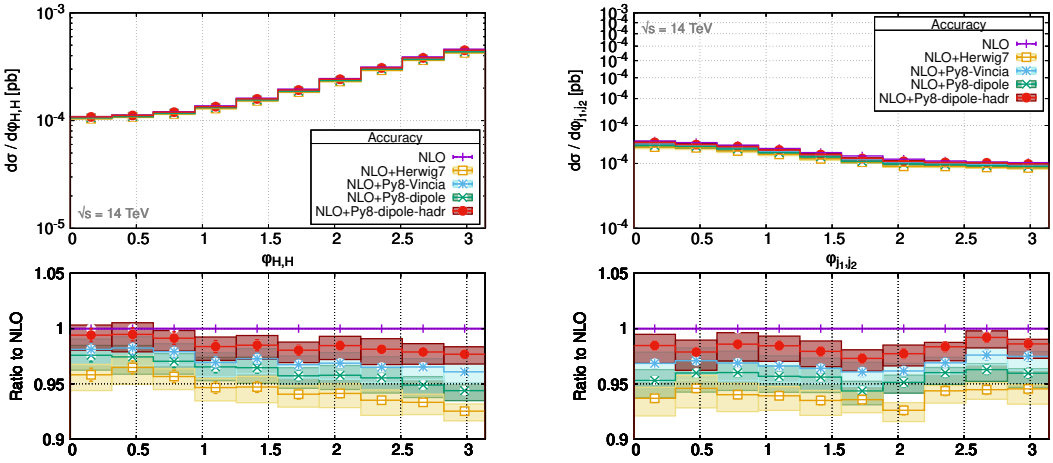

Figure 6: Azimuthal angle separation distributions of the Higgs bosons (left) and the two taggings jets (right) for the VBF HH process as described in the text within the **VBF cut** setup at NLO (purple) and at NLO+PS accuracy using HERWIG7 (orange) or PYTHIA8 with the dipole shower without (green) and with (red) hadronisation/underlying event effects, and the Vincia shower (blue). Their ratios to the respective NLO results are shown in the lower panels. Error bars indicate statistical uncertainties, uncertainty bands correspond to a 7-point variation around the central scale μ_0 of each curve.

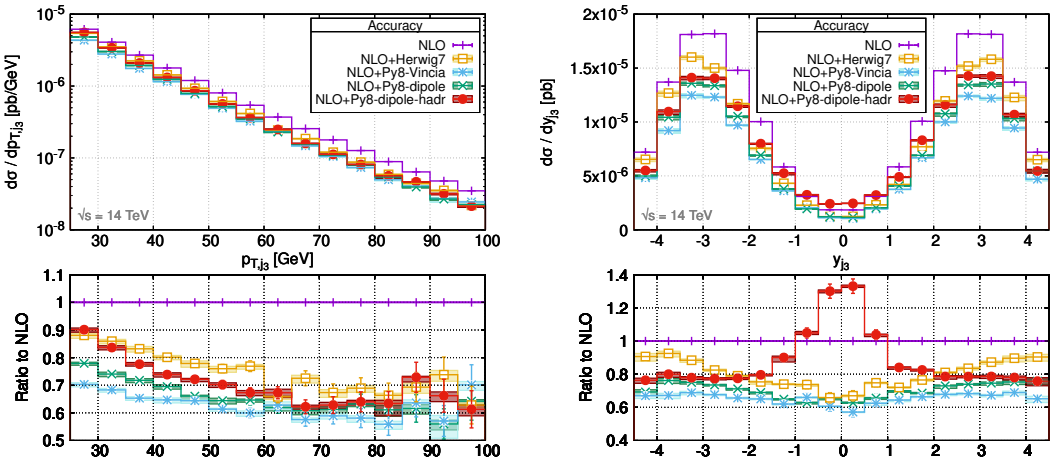

Figure 7: Transverse momentum (left) and rapidity distributions (right) of the third jet for the VBF HH process as described in the text within the **VBF cut** setup. The third jet is required to fulfill the cuts of Eq. (10). Results are shown at NLO (purple) and at NLO+PS accuracy using HERWIG7 (orange) or PYTHIA8 with the dipole shower without (green) and with (red) hadronisation/underlying event effects, and the Vincia shower (blue). Their ratios to the respective NLO results are shown in the lower panels. Error bars indicate statistical uncertainties, uncertainty bands correspond to a 7-point variation around the central scale μ_0 of each curve.

the central-rapidity region tends to be significantly more populated.

5 Conclusions

In this paper we have presented a systematic comparison of two tools for the simulation of the VBF HH process at the LHC and HL-LHC. The two tools differ mainly in what contributions they include – in particular GoSam+Whizard includes LO and NLO-QCD matrix elements for the full EW $HHjj$ final state without resorting to any approximations. The POWHEG-BOX on the other hand resorts to the simpler VBF approximation. We found that for scenarios that are typically used in VBF analyses, and which are designed to suppress contributions beyond the VBF approximation, these tools provide similar predictions at LO and NLO-QCD accuracy both within the SM and in the presence of anomalous Higgs couplings. However, for more inclusive cuts the two predictions start to differ as expected.

This highlights the complementarity of the GoSam+Whizard and POWHEG-BOX for more general applications: GoSam+Whizard includes the full LO and NLO-QCD matrix elements which is of relevance in inclusive selection scenarios. In principle, NLO results matched to a parton shower can also be obtained, but we leave this to future work. The POWHEG-BOX implementation instead uses the VBF approximation but includes an interface to PS generators such as PYTHIA or HERWIG using the POWHEG formalism and thus directly provides NLO+PS results.

Acknowledgements

This work was done on behalf of the LHC Higgs Working Group. The research of PB, GH and MH is supported by the Deutsche Forschungsgemeinschaft (DFG, German Research Foundation) under grant 396021762 - TRR 257. JB is supported in parts by the Federal Ministry of Technology and Space (BMFTR) under grant number 05H24VKB. The authors also acknowledge support by the state of Baden-Württemberg through bwHPC and the DFG through grant no INST 39/963-1 FUGG.

References

[1] ATLAS Collaboration, *Observation of a new particle in the search for the Standard Model Higgs boson with the ATLAS detector at the LHC*, Phys. Lett. B **716**, 1 (2012), doi:10.1016/j.physletb.2012.08.020, 1207.7214.

[2] CMS Collaboration, *Observation of a New Boson at a Mass of 125 GeV with the CMS Experiment at the LHC*, Phys. Lett. B **716**, 30 (2012), doi:10.1016/j.physletb.2012.08.021, 1207.7235.

[3] *High-Luminosity Large Hadron Collider (HL-LHC): Technical Design Report V. 0.1* **4/2017** (2017), doi:10.23731/CYRM-2017-004.

[4] M. Cepeda *et al.*, *Report from Working Group 2: Higgs Physics at the HL-LHC and HE-LHC*, CERN Yellow Rep. Monogr. **7**, 221 (2019), doi:10.23731/CYRM-2019-007.221, 1902.00134.

[5] T. Figy, *Next-to-leading order QCD corrections to light Higgs Pair production via vector boson fusion*, Mod. Phys. Lett. A **23**, 1961 (2008), doi:10.1142/S0217732308028181, 0806.2200.

[6] J. Baglio, A. Djouadi, R. Gröber, M. M. Mühlleitner, J. Quevillon and M. Spira, *The measurement of the Higgs self-coupling at the LHC: theoretical status*, JHEP **04**, 151 (2013), doi:10.1007/JHEP04(2013)151, 1212.5581.

[7] R. Frederix, S. Frixione, V. Hirschi, F. Maltoni, O. Mattelaer, P. Torrielli, E. Vryonidou and M. Zaro, *Higgs pair production at the LHC with NLO and parton-shower effects*, Phys. Lett. B **732**, 142 (2014), doi:10.1016/j.physletb.2014.03.026, 1401.7340.

[8] K. Arnold *et al.*, *VBFNLO: A Parton level Monte Carlo for processes with electroweak bosons*, Comput. Phys. Commun. **180**, 1661 (2009), doi:10.1016/j.cpc.2009.03.006, 0811.4559.

[9] J. Baglio *et al.*, *VBFNLO: A parton level Monte Carlo for processes with electroweak bosons – Manual for Version 3.0* (2011), 1107.4038.

[10] J. Baglio *et al.*, *Release note: VBFNLO 3.0*, Eur. Phys. J. C **84**(10), 1003 (2024), doi:10.1140/epjc/s10052-024-13336-x, 2405.06990.

[11] J. Alwall, R. Frederix, S. Frixione, V. Hirschi, F. Maltoni, O. Mattelaer, H. S. Shao, T. Stelzer, P. Torrielli and M. Zaro, *The automated computation of tree-level and next-to-leading order differential cross sections, and their matching to parton shower simulations*, JHEP **07**, 079 (2014), doi:10.1007/JHEP07(2014)079, 1405.0301.

[12] L.-S. Ling, R.-Y. Zhang, W.-G. Ma, L. Guo, W.-H. Li and X.-Z. Li, *NNLO QCD corrections to Higgs pair production via vector boson fusion at hadron colliders*, Phys. Rev. D **89**(7), 073001 (2014), doi:10.1103/PhysRevD.89.073001, 1401.7754.

[13] F. A. Dreyer and A. Karlberg, *Vector-Boson Fusion Higgs Pair Production at N^3LO*, Phys. Rev. D **98**(11), 114016 (2018), doi:10.1103/PhysRevD.98.114016, 1811.07906.

[14] F. A. Dreyer and A. Karlberg, *Fully differential Vector-Boson Fusion Higgs Pair Production at Next-to-Next-to-Leading Order*, Phys. Rev. D **99**(7), 074028 (2019), doi:10.1103/PhysRevD.99.074028, 1811.07918.

[15] F. A. Dreyer, A. Karlberg and L. Tancredi, *On the impact of non-factorisable corrections in VBF single and double Higgs production*, JHEP **10**, 131 (2020), doi:10.1007/JHEP10(2020)131, [Erratum: JHEP 04, 009 (2022)], 2005.11334.

[16] A. Karlberg, *provbfhh*, https://github.com/alexanderkarlberg/proVBFH.

[17] F. A. Dreyer, A. Karlberg, J.-N. Lang and M. Pellen, *Precise predictions for double-Higgs production via vector-boson fusion*, Eur. Phys. J. C **80**(11), 1037 (2020), doi:10.1140/epjc/s10052-020-08610-7, 2005.13341.

[18] L.-S. Ling, R.-Y. Zhang, W.-G. Ma, X.-Z. Li, L. Guo and S.-M. Wang, *Dimension-six operators in Higgs boson pair production via vector-boson fusion at the LHC*, Phys. Rev. D **96**(5), 055006 (2017), doi:10.1103/PhysRevD.96.055006, 1708.04785.

[19] E. Arganda, C. Garcia-Garcia and M. J. Herrero, *Probing the Higgs self-coupling through double Higgs production in vector boson scattering at the LHC*, Nucl. Phys. B **945**, 114687 (2019), doi:10.1016/j.nuclphysb.2019.114687, 1807.09736.

[20] J. Y. Araz, S. Banerjee, R. S. Gupta and M. Spannowsky, *Precision SMEFT bounds from the VBF Higgs at high transverse momentum*, JHEP **04**, 125 (2021), doi:10.1007/JHEP04(2021)125, 2011.03555.

[21] W. Kilian, S. Sun, Q.-S. Yan, X. Zhao and Z. Zhao, *Multi-Higgs boson production and unitarity in vector-boson fusion at future hadron colliders*, Phys. Rev. D **101**(7), 076012 (2020), doi:10.1103/PhysRevD.101.076012, 1808.05534.

[22] C. Englert, W. Naskar and D. Sutherland, *BSM patterns in scalar-sector coupling modifiers*, JHEP **11**, 158 (2023), doi:10.1007/JHEP11(2023)158, 2307.14809.

[23] A. Dedes, J. Rosiek and M. Ryczkowski, *Double Higgs boson production via vector boson fusion in SMEFT*, Phys. Rev. D **112**(5), 055044 (2025), doi:10.1103/bywd-2dy1, 2506.12917.

[24] R. Gómez-Ambrosio, F. J. Llanes-Estrada, A. Salas-Bernárdez and J. J. Sanz-Cillero, *Distinguishing electroweak EFTs with $W_L W_L \to n h$*, Phys. Rev. D **106**(5), 053004 (2022), doi:10.1103/PhysRevD.106.053004, 2204.01763.

[25] R. Gómez-Ambrosio, F. J. Llanes-Estrada, A. Salas-Bernárdez and J. J. Sanz-Cillero, *SMEFT is falsifiable through multi-Higgs measurements (even in the absence of new light particles)*, Commun. Theor. Phys. **75**(9), 095202 (2023), doi:10.1088/1572-9494/ace95e, 2207.09848.

[26] M. J. Herrero and R. A. Morales, *One-loop corrections for WW to HH in Higgs EFT with the electroweak chiral Lagrangian*, Phys. Rev. D **106**(7), 073008 (2022), doi:10.1103/PhysRevD.106.073008, 2208.05900.

[27] Anisha, D. Domenech, C. Englert, M. J. Herrero and R. A. Morales, *Bosonic multi-Higgs correlations beyond leading order*, Phys. Rev. D **110**(9), 095016 (2024), doi:10.1103/PhysRevD.110.095016, 2405.05385.

[28] Anisha, D. Domenech, C. Englert, M. J. Herrero and R. A. Morales, *HEFT's appraisal of triple (versus double) Higgs weak boson fusion*, Phys. Rev. D **111**(5), 055004 (2025), doi:10.1103/PhysRevD.111.055004, 2407.20706.

[29] D. Domenech, M. Herrero, R. A. Morales and A. Salas-Bernárdez, *Matching HEFT and SMEFT in double and triple Higgs production from weak boson fusion* (2025), 2506.21716.

[30] B. Jäger, A. Karlberg and S. Reinhardt, *Precision tools for the simulation of double-Higgs production via vector-boson fusion*, JHEP **06**, 022 (2025), doi:10.1007/JHEP06(2025)022, 2502.09112.

[31] J. Braun, P. Bredt, G. Heinrich and M. Höfer, *Double Higgs production in vector boson fusion at NLO QCD in HEFT*, JHEP **07**, 209 (2025), doi:10.1007/JHEP07(2025)209, 2502.09132.

[32] M. Ciccolini, A. Denner and S. Dittmaier, *Electroweak and QCD corrections to Higgs production via vector-boson fusion at the LHC*, Phys. Rev. D **77**, 013002 (2008), doi:10.1103/PhysRevD.77.013002, 0710.4749.

[33] T. Figy, C. Oleari and D. Zeppenfeld, *Next-to-leading order jet distributions for Higgs boson production via weak boson fusion*, Phys. Rev. D **68**, 073005 (2003), doi:10.1103/PhysRevD.68.073005, hep-ph/0306109.

[34] F. Feruglio, *The Chiral approach to the electroweak interactions*, Int. J. Mod. Phys. A **8**, 4937 (1993), doi:10.1142/S0217751X93001946, hep-ph/9301281.

[35] J. Bagger, V. D. Barger, K.-m. Cheung, J. F. Gunion, T. Han, G. A. Ladinsky, R. Rosenfeld and C. P. Yuan, *The Strongly interacting W W system: Gold plated modes*, Phys. Rev. D **49**, 1246 (1994), doi:10.1103/PhysRevD.49.1246, hep-ph/9306256.

[36] C. P. Burgess, J. Matias and M. Pospelov, *A Higgs or not a Higgs? What to do if you discover a new scalar particle*, Int. J. Mod. Phys. A **17**, 1841 (2002), doi:10.1142/S0217751X02009813, hep-ph/9912459.

[37] B. Grinstein and M. Trott, *A Higgs-Higgs bound state due to new physics at a TeV*, Phys. Rev. D **76**, 073002 (2007), doi:10.1103/PhysRevD.76.073002, 0704.1505.

[38] R. Alonso, M. B. Gavela, L. Merlo, S. Rigolin and J. Yepes, *The Effective Chiral Lagrangian for a Light Dynamical "Higgs Particle"*, Phys. Lett. B **722**, 330 (2013), doi:10.1016/j.physletb.2013.04.037, [Erratum: Phys.Lett.B 726, 926 (2013)], 1212.3305.

[39] G. Buchalla and O. Cata, *Effective Theory of a Dynamically Broken Electroweak Standard Model at NLO*, JHEP **07**, 101 (2012), doi:10.1007/JHEP07(2012)101, 1203.6510.

[40] G. Buchalla, O. Catà and C. Krause, *Complete Electroweak Chiral Lagrangian with a Light Higgs at NLO*, Nucl. Phys. B **880**, 552 (2014), doi:10.1016/j.nuclphysb.2014.01.018, [Erratum: Nucl.Phys.B 913, 475–478 (2016)], 1307.5017.

[41] W. Buchmüller and D. Wyler, *Effective Lagrangian Analysis of New Interactions and Flavor Conservation*, Nucl. Phys. B **268**, 621 (1986), doi:10.1016/0550-3213(86)90262-2.

[42] B. Grzadkowski, M. Iskrzynski, M. Misiak and J. Rosiek, *Dimension-Six Terms in the Standard Model Lagrangian*, JHEP **10**, 085 (2010), doi:10.1007/JHEP10(2010)085, 1008.4884.

[43] I. Brivio and M. Trott, *The Standard Model as an Effective Field Theory*, Phys. Rept. **793**, 1 (2019), doi:10.1016/j.physrep.2018.11.002, 1706.08945.

[44] G. Isidori, F. Wilsch and D. Wyler, *The standard model effective field theory at work*, Rev. Mod. Phys. **96**(1), 015006 (2024), doi:10.1103/RevModPhys.96.015006, 2303.16922.

[45] M. J. G. Veltman, *Limit on Mass Differences in the Weinberg Model*, Nucl. Phys. B **123**, 89 (1977), doi:10.1016/0550-3213(77)90342-X.

[46] S. Navas *et al.*, *Review of particle physics*, Phys. Rev. D **110**(3), 030001 (2024), doi:10.1103/PhysRevD.110.030001.

[47] C. Degrande, G. Durieux, F. Maltoni, K. Mimasu, E. Vryonidou and C. Zhang, *Automated one-loop computations in the standard model effective field theory*, Phys. Rev. D **103**(9), 096024 (2021), doi:10.1103/PhysRevD.103.096024, 2008.11743.

[48] K. Hagiwara, S. Ishihara, R. Szalapski and D. Zeppenfeld, *Low-energy effects of new interactions in the electroweak boson sector*, Phys. Rev. D **48**, 2182 (1993), doi:10.1103/PhysRevD.48.2182.

[49] A. David, A. Denner, M. Duehrssen, M. Grazzini, C. Grojean, G. Passarino, M. Schumacher, M. Spira, G. Weiglein and M. Zanetti, *LHC HXSWG interim recommendations to explore the coupling structure of a Higgs-like particle* (2012), 1209.0040.

[50] G. Cullen, N. Greiner, G. Heinrich, G. Luisoni, P. Mastrolia, G. Ossola, T. Reiter and F. Tramontano, *Automated One-Loop Calculations with GoSam*, Eur. Phys. J. C **72**, 1889 (2012), doi:10.1140/epjc/s10052-012-1889-1, 1111.2034.

[51] G. Cullen *et al.*, *GoSam-2.0: a tool for automated one-loop calculations within the Standard Model and beyond*, Eur. Phys. J. C **74**(8), 3001 (2014), doi:10.1140/epjc/s10052-014-3001-5, 1404.7096.

[52] J. Braun, B. Campillo Aveleira, G. Heinrich, M. Höfer, S. P. Jones, M. Kerner, J. Lang and V. Magerya, *One-Loop Calculations in Effective Field Theories with GoSam-3.0* (2025), 2507.23549.

[53] P. Nogueira, *Automatic Feynman Graph Generation*, J. Comput. Phys. **105**, 279 (1993), doi:10.1006/jcph.1993.1074.

[54] J. A. M. Vermaseren, *New features of FORM* (2000), math-ph/0010025.

[55] J. Kuipers, T. Ueda, J. A. M. Vermaseren and J. Vollinga, *FORM version 4.0*, Comput. Phys. Commun. **184**, 1453 (2013), doi:10.1016/j.cpc.2012.12.028, 1203.6543.

[56] H. van Deurzen, G. Luisoni, P. Mastrolia, E. Mirabella, G. Ossola and T. Peraro, *Multi-leg One-loop Massive Amplitudes from Integrand Reduction via Laurent Expansion*, JHEP **03**, 115 (2014), doi:10.1007/JHEP03(2014)115, 1312.6678.

[57] T. Peraro, *Ninja: Automated Integrand Reduction via Laurent Expansion for One-Loop Amplitudes*, Comput. Phys. Commun. **185**, 2771 (2014), doi:10.1016/j.cpc.2014.06.017, 1403.1229.

[58] A. van Hameren, *OneLOop: For the evaluation of one-loop scalar functions*, Comput. Phys. Commun. **182**, 2427 (2011), doi:10.1016/j.cpc.2011.06.011, 1007.4716.

[59] C. Degrande, C. Duhr, B. Fuks, D. Grellscheid, O. Mattelaer and T. Reiter, *UFO - The Universal FeynRules Output*, Comput. Phys. Commun. **183**, 1201 (2012), doi:10.1016/j.cpc.2012.01.022, 1108.2040.

[60] L. Darmé *et al.*, *UFO 2.0: the "Universal Feynman Output" format*, Eur. Phys. J. C **83**(7), 631 (2023), doi:10.1140/epjc/s10052-023-11780-9, 2304.09883.

[61] W. Kilian, T. Ohl and J. Reuter, *WHIZARD: Simulating Multi-Particle Processes at LHC and ILC*, Eur. Phys. J. C **71**, 1742 (2011), doi:10.1140/epjc/s10052-011-1742-y, 0708.4233.

[62] M. Moretti, T. Ohl and J. Reuter, *O'Mega: An Optimizing matrix element generator* pp. 1981–2009 (2001), hep-ph/0102195.

[63] B. Chokoufé Nejad, W. Kilian, J. M. Lindert, S. Pozzorini, J. Reuter and C. Weiss, *NLO QCD predictions for off-shell $t\bar{t}$ and $t\bar{t}H$ production and decay at a linear collider*, JHEP **12**, 075 (2016), doi:10.1007/JHEP12(2016)075, 1609.03390.

[64] P. Stienemeier, S. Braß, P. Bredt, W. Kilian, N. Kreher, T. Ohl, J. Reuter, V. Rothe and T. Striegl, *WHIZARD 3.0: Status and News*, In *International Workshop on Future Linear Colliders* (2021), 2104.11141.

[65] P. Bredt, J. Reuter and P. Stienemeier, *Automated NLO SM corrections for all colliders*, PoS **ICHEP2022**, 1182 (2022), doi:10.22323/1.414.1182, 2210.07157.

[66] S. Frixione, Z. Kunszt and A. Signer, *Three jet cross-sections to next-to-leading order*, Nucl. Phys. B **467**, 399 (1996), doi:10.1016/0550-3213(96)00110-1, hep-ph/9512328.

[67] P. Nason, *A New method for combining NLO QCD with shower Monte Carlo algorithms*, JHEP **11**, 040 (2004), doi:10.1088/1126-6708/2004/11/040, hep-ph/0409146.

[68] S. Frixione, P. Nason and C. Oleari, *Matching NLO QCD computations with Parton Shower simulations: the POWHEG method*, JHEP **11**, 070 (2007), doi:10.1088/1126-6708/2007/11/070, 0709.2092.

[69] B. Chokoufe Nejad, W. Kilian, J. Reuter and C. Weiss, *Matching NLO QCD Corrections in WHIZARD with the POWHEG scheme*, PoS **EPS-HEP2015**, 317 (2015), doi:10.22323/1.234.0317, 1510.02739.

[70] P. Stienemeier, *Automation and Application of fixed-order and matched NLO Simulations*, Ph.D. thesis, Hamburg U., Hamburg, doi:10.3204/PUBDB-2022-07425 (2022).

[71] T. Binoth *et al.*, *A Proposal for a Standard Interface between Monte Carlo Tools and One-Loop Programs*, Comput. Phys. Commun. **181**, 1612 (2010), doi:10.1016/j.cpc.2010.05.016, 1001.1307.

[72] S. Alioli *et al.*, *Update of the Binoth Les Houches Accord for a standard interface between Monte Carlo tools and one-loop programs*, Comput. Phys. Commun. **185**, 560 (2014), doi:10.1016/j.cpc.2013.10.020, 1308.3462.

[73] S. Alioli, P. Nason, C. Oleari and E. Re, *A general framework for implementing NLO calculations in shower Monte Carlo programs: the POWHEG BOX*, JHEP **06**, 043 (2010), doi:10.1007/JHEP06(2010)043, 1002.2581.

[74] G. Bewick *et al.*, *Herwig 7.3 release note*, Eur. Phys. J. C **84**(10), 1053 (2024), doi:10.1140/epjc/s10052-024-13211-9, 2312.05175.

[75] C. Bierlich *et al.*, *A comprehensive guide to the physics and usage of PYTHIA 8.3*, SciPost Phys. Codeb. **2022**, 8 (2022), doi:10.21468/SciPostPhysCodeb.8, 2203.11601.

[76] R. D. Ball *et al.*, *The PDF4LHC21 combination of global PDF fits for the LHC Run III*, J. Phys. G **49**(8), 080501 (2022), doi:10.1088/1361-6471/ac7216, 2203.05506.

[77] M. Cacciari, G. P. Salam and G. Soyez, *The anti-k_t jet clustering algorithm*, JHEP **04**, 063 (2008), doi:10.1088/1126-6708/2008/04/063, 0802.1189.

[78] A. Biekötter, B. D. Pecjak, D. J. Scott and T. Smith, *Electroweak input schemes and universal corrections in SMEFT*, JHEP **07**, 115 (2023), doi:10.1007/JHEP07(2023)115, 2305.03763.

[79] B. Jager, C. Oleari and D. Zeppenfeld, *Next-to-leading order QCD corrections to W+W- production via vector-boson fusion*, JHEP **07**, 015 (2006), doi:10.1088/1126-6708/2006/07/015, hep-ph/0603177.

[80] M. Cacciari, F. A. Dreyer, A. Karlberg, G. P. Salam and G. Zanderighi, *Fully Differential Vector-Boson-Fusion Higgs Production at Next-to-Next-to-Leading Order*, Phys. Rev. Lett. **115**(8), 082002 (2015), doi:10.1103/PhysRevLett.115.082002, [Erratum: Phys.Rev.Lett. 120, 139901 (2018)], 1506.02660.

[81] ATLAS Collaboration, *Combination of Searches for Higgs Boson Pair Production in pp Collisions at s=13 TeV with the ATLAS Detector*, Phys. Rev. Lett. **133**(10), 101801 (2024), doi:10.1103/PhysRevLett.133.101801, 2406.09971.

[82] CMS Collaboration, *Constraints on the Higgs boson self-coupling from the combination of single and double Higgs boson production in proton-proton collisions at s=13TeV*, Phys. Lett. B **861**, 139210 (2025), doi:10.1016/j.physletb.2024.139210, 2407.13554.

[83] P. Skands, S. Carrazza and J. Rojo, *Tuning PYTHIA 8.1: the Monash 2013 Tune*, Eur. Phys. J. C **74**(8), 3024 (2014), doi:10.1140/epjc/s10052-014-3024-y, 1404.5630.

[84] N. Fischer, S. Prestel, M. Ritzmann and P. Skands, *Vincia for Hadron Colliders*, Eur. Phys. J. C **76**(11), 589 (2016), doi:10.1140/epjc/s10052-016-4429-6, 1605.06142.

[85] B. Jäger, A. Karlberg, S. Plätzer, J. Scheller and M. Zaro, *Parton-shower effects in Higgs production via Vector-Boson Fusion*, Eur. Phys. J. C **80**(8), 756 (2020), doi:10.1140/epjc/s10052-020-8326-7, 2003.12435.

[86] S. Höche, S. Mrenna, S. Payne, C. T. Preuss and P. Skands, *A Study of QCD Radiation in VBF Higgs Production with Vincia and Pythia*, SciPost Phys. **12**(1), 010 (2022), doi:10.21468/SciPostPhys.12.1.010, 2106.10987.